Multi-Objective Performance Selection of Fe-8Cr-3V-2Mo-2W Hardfacing on SCM420 by Directed Energy Deposition with Microstructural Interpretation

William W. Predebon[1,*]

[1] Retired professor and chair of the Department of Mechanical Engineering-Engineering Mechanics, at Michigan Technological University
* Correspondence: w.prebon@gmail.com

Abstract: Directed energy deposition is being widely applied to localized hardfacing, repair, and surface-tailored property improvements for mechanical parts; yet, many tool steel routes are evaluated through isolated hardness maxima or wear resistance peaks irrespective of practical service requirements. The present study aims at selecting the Fe-8Cr-3V-2Mo-2W hardfacing route on SCM420 through a service-driven multi-objective decision-making analysis supplemented with microstructural insights. Four mechanically equivalent surface conditions are considered: carburized SCM420, as-built M2, as-built Fe-8Cr-3V-2Mo-2W, and post-heat-treated Fe-8Cr-3V-2Mo-2W. The process parameters, chemical composition, post-treatment procedure, hardness, wear loss, wear track width, impact energy, tensile strength, and microstructure analysis are grouped into one comprehensive mechanical property matrix based on specific normalization factors, score-decomposition into relative contributions, decision boundary equations, ideal-distance weighted ranking, and robustness metrics. Post-heat treatment boosts Fe-8Cr-3V-2Mo-2W hardness from 48 to 62 HRc, reduces wear loss from 6.33 to 2.32 mg, reduces wear track width from 1030 to 798 µm, and boosts tensile strength from 607 to 922 MPa; yet, post-heat treated Fe-8Cr-3V-2Mo-2W exhibits lower impact energy compared to its as-built condition, decreasing from 11 to 6 J. It means that the Fe-8Cr-3V-2Mo-2W post-heat treatment gain vector is significantly positive in terms of wear and tensile properties; meanwhile, it is negatively affecting impact energy. Application-weighted scores indicate that the as-built M2 tool steel performs better for wear service, whereas the carburized SCM420 steel continues to excel in terms of impact dominance. For a balanced application, the Fe-8Cr-3V-2Mo-2W post-heat treated route emerges as a preferable solution. The decision boundaries and distances-to-ideality confirm that the above statement is not based on artificial numerical manipulations, as the post-treated Fe-8Cr-3V-2Mo-2W route is winning when both tensile capacity and wear resistance are strongly weighted. The study thus suggests Fe-8Cr-3V-2Mo-2W route as a targeted DED hardfacing method for load-bearing wear applications, which require optimal manufacturing processes, microstructure, and mechanical loading.

Keywords: directed energy deposition; hardfacing; tool steel; SCM420; materials selection; wear resistance; surface engineering; manufacturing and production engineering

Citation: William W. Predebon. 2021. Multi-Objective Performance Selection of Fe-8Cr-3V-2Mo-2W Hardfacing on SCM420 by Directed Energy Deposition with Microstructural Interpretation. *TK Techforum Journal (ThyssenKrupp Techforum)* 2021(2): 52–69.

Received: May-08-2020
Accepted: July-27-2021
Published: Sptember-30-2021

1. Introduction

Surface degradation continues to be one of the major reasons for mechanical performance degradation of the materials undergoing sliding, rolling, impacting, or cyclic contact. Gears, dies, shafts, valve seats, form tools, molding inserts, railway contact components, and refurbished machine parts seldom fail because the entire volume of the material suffers uniform loss of strength. On the contrary, degradation usually starts at the level of the subsurface region where, owing to repeated frictional interactions, plastic deformation, thermal cycles, oxidation, spallation, adhesion or abrasive grooving, the stress state is formed which is significantly different from that of the core material. Surface carburizing

and similar types of case hardening are still highly valued because they enable to build up a wear-resistant surface reinforced with a tougher interior. However, modern mechanical systems are increasingly requiring localized repair, alloy-selective overlays, or property-tuned surfaces which cannot be accomplished solely by means of bulk treatment or classical case hardening [1–3].

Among the available techniques for such tasks, directed energy deposition (DED) stands out in view of its versatility and flexibility. During a DED operation, a focused laser beam melts a spot on the substrate surface into a melt pool into which a metal powder or wire is fed, thus forming a deposited material layer. Depending on the particular requirements of a mechanical system, a DED operation could rebuild lost geometry, form a wear-resistant overlay, or fabricate a functionally graded surface coating only in those areas where reinforcement is needed. While being less selective than the traditional surface treatments, DED provides better selectivity and larger thicknesses as compared to conventional surface treatments. Meanwhile, compared with standard welding techniques, it allows a better control over track placement, feed rate, melting process, and composition of the deposited layer. Hence the growing attention to DED for repair and material-tailored applications of mechanical components [4–7].

When it comes to hardfacing, however, the utility of DED cannot be assessed solely on account of precision and deposition accuracy. Hardness, martensite content, dilution ratio, remelted interfaces, post-processing, and heat treatments are just some of the factors that affect the mechanical properties of a deposited Fe layer, i.e., martensite presence, austenite retention, primary carbide precipitation, eutectic carbide precipitation, tempering martensite transformation, and composite microstructures. Tool steels and carbide-forming ferritic Fe alloys exhibit high hardness and wear-resistance thanks to the presence of hardening phases and carbon-rich compounds. However, at the same time, they are prone to crack formation and are characterized by brittle failure modes and low fracture tolerance. Thus, the challenge is not to produce a surface deposit which is as hard as possible but to make sure it meets specific demands of a mechanical component in terms of wear, tensile capacity, and fracture tolerance [8–11].

One of the weaknesses of existing hardfacing studies is that they frequently evaluate various options based on single mechanical properties. The hardness or wear resistance, for example, of one material may exceed those of others, thus favoring the former in the comparative analysis. Yet a repaired shaft shoulder, a die insert, a carburized gear element, and a guiding surface do not share the same performance criteria. Their failure criteria are also different: while for one the key failure mode may be wearing out, for another it might be sudden fracturing and for the next one insufficient strength under compressive loads after repair. Material choice theory and multi-objective analysis are helpful in resolving the issue since they involve interpreting each measured property in the context of specific application goals [12–14].

From this point of view, the Fe-8Cr-3V-2Mo-2W hardfacing system deposited onto SCM420 steel becomes quite suitable for multi-objective route evaluation. The Jeong et al. Fe-8Cr-3V-2Mo-2W/SCM420 dataset encompasses four materials – a carburized SCM420 steel, as-built M2 steel, as-built Fe-8Cr-3V-2Mo-2W alloy, and Fe-8Cr-3V-2Mo-2W alloy processed via post-heating treatment [15]. The property trends described in the paper are inherently multiple. Heat treatment enhances Fe-8Cr-3V-2Mo-2W hardness and ultimate tensile strength but also decreases the wear-resistance. Conversely, as-built M2 displays good wear-resistance, while a carburized SCM420 shows higher impact tolerance than any of the remaining three materials considered. This does not provide a universal criterion of superiority but creates room for multi-objective decision making.

Indeed, it is worth considering the metallurgy of the Fe-8Cr-3V-2Mo-2W alloy to appreciate the importance of service-oriented analysis. High carbon steels and high-speed tool steels can exhibit high hardness due to carbide dispersion, secondary hardening, reduction in retained austenite, or tempering. At the same time, they tend to develop a coarse and brittle martensite matrix, carbide network structures, and porous defects, thus

compromising fracture tolerance. DED studies of recent years on Fe carbide-forming high-speed and high-carbon steels reveal that heat treatment enhancing the hardness or wear resistance can significantly change their fracture properties as well [16–18]. Equation-based route ranking procedure seems to be more appropriate here.

The route-selection analysis consists of several consecutive steps including property matrix creation, dimensional properties conversion into desirabilities, decomposition of criterion-based scores, construction of decision-boundary equations, and weighted distance to ideal diagnostics. The discussion of the results reveals links between numerical outcomes and observed microstructures and fracture modes, thus providing additional insights into application possibilities of the analyzed materials.

2. Materials and Methods

2.1. Analytical basis and mechanical-property matrix

This section presents the analytical basis for the comparison route selection process. This includes an overview of the Fe-8Cr-3V-2Mo-2W deposition dataset of Jeong et al. as applied to SCM420, which consists of a consistent set of manufacturing, microstructural, and mechanical values corresponding to four directly comparable surface conditions: carburized SCM420, as-built M2 deposited by DED, as-built Fe-8Cr-3V-2Mo-2W deposited by DED, and post-heat-treated Fe-8Cr-3V-2Mo-2W deposited by DED. These values are arranged into a mechanical-property matrix.

Table 1 summarizes the DED manufacturing conditions used in generating the Fe-8Cr-3V-2Mo-2W deposit compared against the other materials. The deposition method used a direct metal tooling deposition platform equipped with a 4 kW CO_2 laser and a laser beam diameter of 1 mm, though the particular DED conditions used to create the deposit in question were a laser power of 800 W, scanning speed of 850 mm/min, powder feed rate of 5 g/min, 8.0 L/min coaxial gas flow, and 2.5 L/min shielding gas flow.

Table 1. DED manufacturing conditions used for the compared deposited specimens.

Laser power (W)	Scanning speed (mm/min)	Powder feed rate (g/min)	Coaxial gas (L/min)	Shielding gas (L/min)
800	850	5.0	8.0	2.5

Table 2 presents the chemical compositions of the Fe-8Cr-3V-2Mo-2W powder material, the comparison M2 powder, and the SCM420 substrate. Fe-8Cr-3V-2Mo-2W is of relevance to this analysis due to its significant carbon, chromium, vanadium, molybdenum, and tungsten content, all of which indicate the potential for phase transformation and carbide formation in the deposition and subsequent heat treatment.

Table 2. Chemical composition of the materials used in the compiled dataset (wt%).

Material	C	Si	Mn	Mo	Cr	V	W	P	S	Ni	Cu
Fe-8Cr-3V-2Mo-2W powder	1.08	1.38	0.34	1.86	7.80	2.66	1.73	–	–	–	–
AISI M2 powder	0.803	0.16	0.29	4.84	3.98	0.90	5.84	0.018	0.013	0.07	–
SCM420 substrate	0.19	0.23	0.80	0.17	1.00	–	–	–	–	0.02	0.02

Table 3 shows the post-deposition heat-treatment steps performed on the Fe-8Cr-3V-2Mo-2W deposit. It is important to note that the most significant differences between the as-built and post-heat-treated Fe-8Cr-3V-2Mo-2W surfaces derive from this process.

Figure 1 shows the numerical DED parameters within their actual manufacturing context. The image demonstrates the localized laser-material interaction resulting in a metallurgically bonded hardfacing layer on the substrate. This figure is used here in order to clarify how the DED process parameters in Table 1 relate to deposited layer formation.

In doing so, the figure reveals that the decision-making task starts at the layer creation level, and not at that of alloy selection. The thermal condition of the melt pool – and consequently, the phase structure upon cooling – is defined by the laser power, scanning speed, powder delivery, shielding gas, and substrate dilution values.

Figure 2 illustrates the heat treatment process flow in Table 3. Pre-austenitizing prepares the deposited layer for austenitizing, oil quenching leads to high hardness in the transformed layer, while repeated tempering ensures that excessive brittleness is minimized, and carbide strengthening becomes enhanced. Figure 2 is thus more than just illustrative; it shows the thermal processing required to determine the changes observed after heat treatment, presented in Table 7.

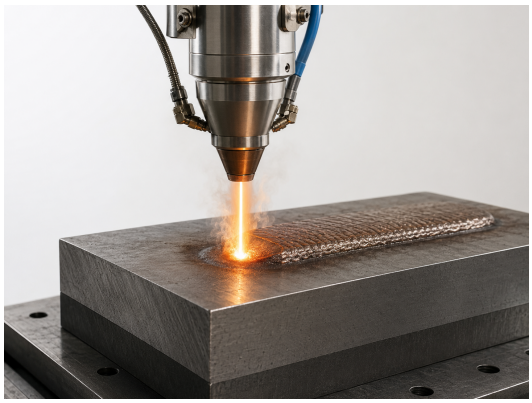

Figure 1. Directed energy deposition track formation on the SCM420 substrate. The figure illustrates the localized melting condition of the material achieved by the DED parameters presented in Table 1; the created deposited layer forms the base for as-built M2 and Fe-8Cr-3V-2Mo-2W conditions comparisons.

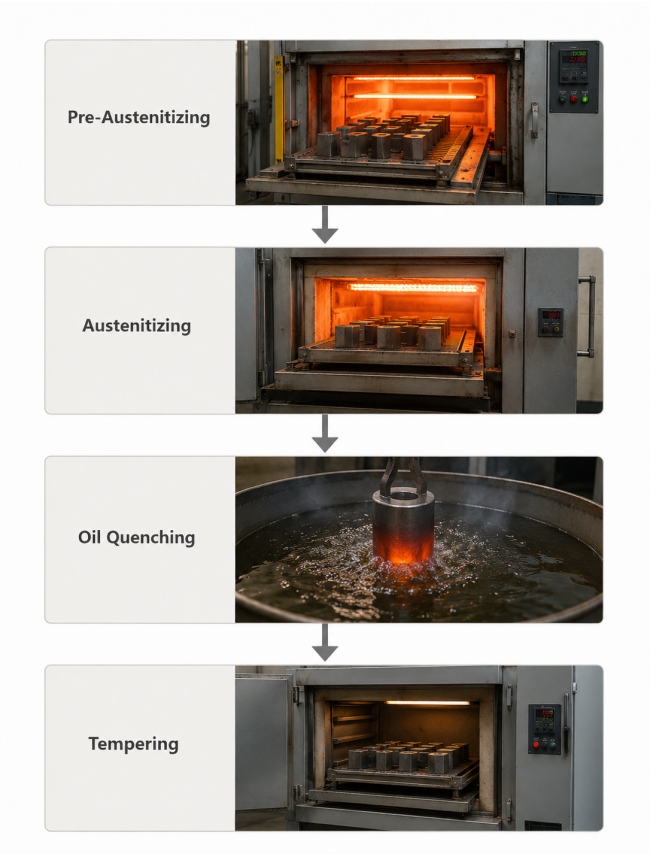

Figure 2. Heat-treatment sequence for the post-deposited Fe-8Cr-3V-2Mo-2W layer. The four-step process involves pre-austenitizing, austenitizing, oil quenching, and repeated tempering. The resultant metal is referred to as Fe-8Cr-3V-2Mo-2W + PHT.

Table 3. Post-deposition heat-treatment schedule used for Fe-8Cr-3V-2Mo-2W.

Step	Condition
Pre-austenitizing	840 °C for 2 h in a nitrogen-purged chamber
Austenitizing	1060 °C for 40–45 min
Quenching	Oil quenching at 2 bar
Tempering	Air cooling at 520 °C for 2 h, repeated three times

The representation of the thermal process independently serves to distinguish the post-heat treatment sample from the as-deposited Fe-8Cr-3V-2Mo-2W process route. It is an entirely new state that results from controlled phase transformation and tempering processes, hence the considerable differences between the hardness, wear performance, tensile strength, and impact energy of Fe-8Cr-3V-2Mo-2W + PHT and as-deposited Fe-8Cr-3V-2Mo-2W.

2.2. Properties Matrix

The properties matrix can be seen in Table 4. There are four main criteria chosen, which include hardness of the surface, wear loss, absorbed impact energy, and tensile strength. The reason behind choosing those is that they have comparable data available for all the suggested routes. Another parameter used is the width of the wear track, which supports the tribology criteria.

Table 4. Mechanical-property matrix used for route selection.

Surface condition	Hardness (HRc)	Wear loss (mg)	Wear track (μm)	Impact energy (J)	Tensile (MPa)
C-SCM420	60	5.00	814	60.5	877
As-built M2	64	0.30	660	25.0	592
As-built Fe-8Cr-3V-2Mo-2W	48	6.33	1030	11.0	607
Fe-8Cr-3V-2Mo-2W + PHT	62	2.32	798	6.0	922

The findings from each of the conditions are summarized in Table 5. It should be noted that this table does not influence any calculation of scores; rather, its purpose lies in illustrating the underlying metallurgical evidence of phase constitution, carbide presence, failure mode, and load-bearing capability.

Table 5. Phase constitution and microstructure details for ranking interpretation.

Condition	Microstructure / phase evidence	Likely property consequence
C-SCM420	Carburizing layer, diffusion zone, and base zone; high-carbon martensite containing retained austenite; ductility of substrate aids plasticity.	High impact energy absorption capacity and solid tensile capacity due to case-core microstructure; wear begins upon breaking through the thin carburizing layer.
As-built M2	Columnar dendrites adjacent to the interface and equiaxial crystals at the core; martensite within an austenitic matrix; rod- and sphere-shaped carbides rich in tungsten; peak tungsten carbide content.	Very high hardness and superior wear resistance due to the complex carbide structure; some toughness is maintained through the fracture pattern.
As-built Fe-8Cr-3V-2Mo-2W	Peak values of austenite and martensite only; larger grain size compared with M2; small spherical and rod-shaped chromium carbides; relatively high proportion of retained austenite.	Weakest overall combination because hardness, wear resistance, and strength are low prior to secondary hardening.
Fe-8Cr-3V-2Mo-2W + PHT	Decreased proportion of retained austenite, increased martensite and tempered martensite after triple tempering; agglomerated eutectic chromium carbides at grain boundaries.	Significantly improved hardness, wear resistance, and tensile strength, but reduced impact energy absorption due to increased brittleness.

The conceptual microstructure–property mechanism map of the four considered surface states is shown in Figure 3. This map incorporates the concepts of phase constitution and morphological characteristics in addition to the mechanisms of mechanical strengthening that underlie the observed performance trends. In the case of the carburized SCM420 steel surface state, the mechanism map focuses on the classical concept of case-core structure with the wear-resistant martensitic and carbon-enriched surface layer and the stronger

low-carbon core capable of bearing loads without failing. On the contrary, the as-built M2 surface state features the wear-oriented microstructure, which includes the high content of primary and secondary carbides in a hard matrix, ensuring high abrasion resistance at the expense of possible decrease in toughness due to microstructural brittleness.

The retained austenite-rich microstructure characterizes the as-built Fe–8Cr–3V–2Mo –2W system owing to its rapid solidification and incomplete transformation. This microstructure leads to increased ductility; however, it ensures relatively low hardness and wear resistance. Under post-heat-treatment, Fe–8Cr–3V–2Mo–2W becomes strengthened via transformation to the martensite- and carbide-containing microstructure, when the amount of retained austenite becomes minimal, and the fine dispersion of carbides takes place in the martensite matrix. This microstructure combines good mechanical properties in terms of hardness, wear resistance, and strength, but retains a sufficient level of toughness. Overall, the mechanism map demonstrates how the processes of microstructure formation lead to observed mechanical properties.

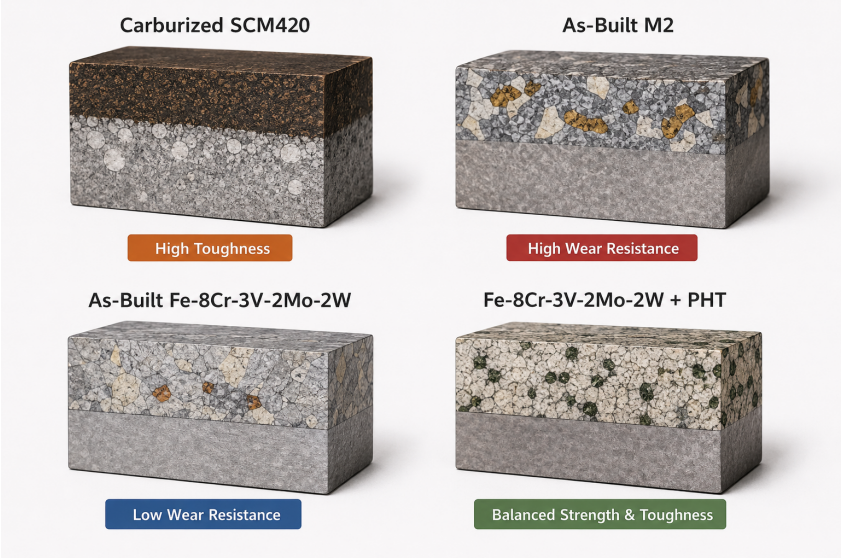

Figure 3. Conceptual microstructure–property mechanism map for the four compared surface conditions. The schematic reveals the case-core microstructure in carburized SCM420, the carbide-rich wear-oriented microstructure of as-built M2, the retained-austenite-rich as-built Fe-8Cr-3V-2Mo-2W, and the martensite- and carbide-rich microstructure of post-heat-treated Fe-8Cr-3V-2Mo-2W.

As can be seen from Figure 3, the microstructural characteristics can now be linked to the numerical ranking obtained previously, as the toughening, wear-resistance, weak as-built, and heat-treatment strengthening effects can be easily distinguished. It means that the obtained desirability values represent the consequence of certain phase constitution and morphology, and not just the arbitrary numbers.

2.3. Normalization, contribution analysis, and decision criteria

Since the retained criteria differ from each other in units and optimization direction, hardness, impact energy, and tensile strength are defined as beneficial responses, whereas wear loss is treated as a cost response, where smaller values correspond to improvement in material performance. Consequently, each property was converted into a dimensionless desirability value z_{ij} for candidate i and criterion j. For beneficial criteria, the conversion was

$$z_{ij} = \frac{x_{ij} - x_j^{\min}}{x_j^{\max} - x_j^{\min}}, \tag{1}$$

and for the wear-loss criterion it was

$$z_{ij} = \frac{x_j^{\max} - x_{ij}}{x_j^{\max} - x_j^{\min}}. \tag{2}$$

The benefit and cost criteria in Eqs. (1) and (2) have been put on an identical scale ranging between 0 and 1, where a score of 1 indicates the best candidate in the current evaluation group and a score of 0 denotes the worst candidate under the same criterion. These values should be considered as part of the selection criteria scale and not the materials' property scale.

Table 6 presents the numerical values employed in the normalization process. This table makes the computation process obvious. For instance, the normalized value of tensile strength ranges between a span of 330 MPa while the impact desirability is normalized using a span of 54.5 J. Consequently, a small numerical change in normalized impact desirability can correspond to a physically large change in absorbed energy.

Table 6. Normalization constants used to convert measured properties into dimensionless desirability values.

Criterion	Optimization	Minimum	Maximum	Range
Hardness (HRc)	Larger is better	48	64	16
Wear loss (mg)	Smaller is better	0.30	6.33	6.03
Impact energy (J)	Larger is better	6.0	60.5	54.5
Tensile strength (MPa)	Larger is better	592	922	330

The overall score of candidate i according to the weighted-sum model was computed by Eq. (3)

$$S_i = \sum_{j=1}^{m} w_j z_{ij}, \tag{3}$$

subject to

$$\sum_{j=1}^{m} w_j = 1, \tag{4}$$

where w_j is the design weight for criterion j and $m = 4$. Eq. (3) is chosen due to its simplicity and physical interpretation: each property contributes to the overall score in direct proportion to both normalized property performance and the service importance of this property. Constraint (4) ensures that the scores remain bounded and comparable within duty cases.

To avoid the presentation of the weighted score as a black-box value, the contribution of the criterion to the total score was additionally calculated as

$$q_{ij} = w_j z_{ij}, \qquad S_i = q_{iH} + q_{iW} + q_{iI} + q_{iT}, \tag{5}$$

where H, W, I, and T stand for hardness, wear desirability, impact energy, and tensile strength, respectively. Eq. (5) is helpful since it allows checking whether the good score is driven by one property or by the combination of several properties.

The pairwise ranking margins have been calculated by

$$\Delta S_{A-B} = S_A - S_B = \sum_{j=1}^{m} w_j (z_{Aj} - z_{Bj}). \tag{6}$$

If the value ΔS_{A-B} is positive, this indicates that route A outranks route B under the chosen set of weights. Since the formula for ranking margins is presented explicitly, it can be used to establish the decision boundary by identifying which weights must be applied to the strength, wear, hardness, or impact in order to change the ranking.

In addition to this analysis, the weighted distance to the ideal solution has been calculated as a diagnostic tool. The positive ideal vector is $z_j = 1$ for all criteria and the negative ideal vector is $z_j = 0$ for all criteria. The weighted distances to the reference points were calculated as follows:

$$d_i^+ = \left[\sum_{j=1}^{m} w_j (1 - z_{ij})^2\right]^{1/2}, \tag{7}$$

$$d_i^- = \left[\sum_{j=1}^{m} w_j z_{ij}^2\right]^{1/2}, \tag{8}$$

and the relative closeness index was calculated as

$$C_i = \frac{d_i^-}{d_i^+ + d_i^-}. \tag{9}$$

Eqs. (7)–(9) do not replace the weighted-sum ranking; rather, they test whether the preferred candidate is also closer to an ideal profile in the weighted property space. This is useful in a small dataset because it helps distinguish a robust preference from a ranking caused by one isolated score component [14,19–21].

2.4. Weights of applications and ranking criteria

Three service conditions were identified to distinguish different categories of mechanical use:

1. *Tooling susceptible to wear*: $w_H = 0.30$, $w_W = 0.50$, $w_I = 0.10$, $w_T = 0.10$.
2. *Component susceptible to impact*: $w_H = 0.10$, $w_W = 0.10$, $w_I = 0.60$, $w_T = 0.20$.
3. *Structural hardfacing with wear resistance*: $w_H = 0.25$, $w_W = 0.35$, $w_I = 0.10$, $w_T = 0.30$.

These values denote priorities rather than any universal constants: the first condition requires emphasis on the abrasion and wear resistance aspects, the second emphasizes ability to handle impact loading, and the third is an example of a deposited overlay that needs to withstand wear but also endure considerable static or quasi-static load. It is therefore logical to expect that under the same conditions of measured properties, different preferred paths may be identified, as one would naturally expect from the service-driven approach to material selection.

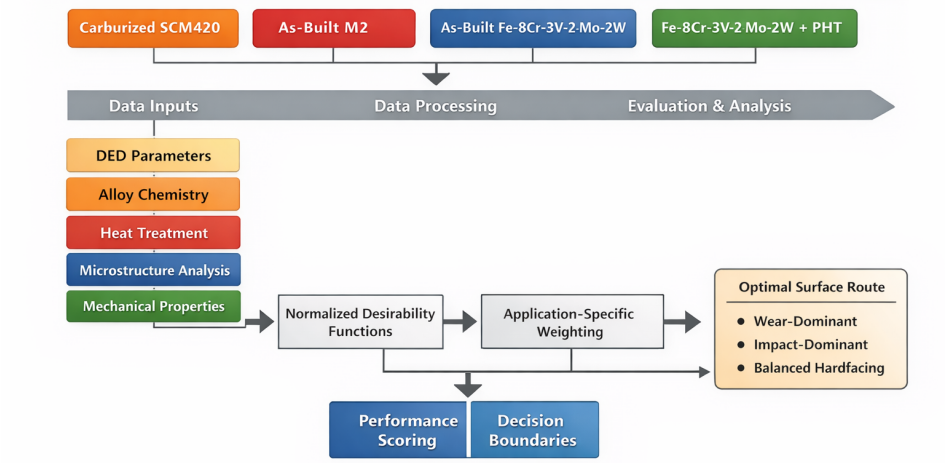

Figure 4. Multi-objective ranking sequence for the Fe-8Cr-3V-2Mo-2W/SCM420 hardfacing comparison. DED parameters, alloy chemistry, heat treatment, microstructural features, and measured properties of deposited overlays are used to convert each manufacturing route into a normalized desirability function and application-specific score subject to decision boundaries.

All the steps of calculation and interpretation are listed schematically in Figure 4. From process and chemistry data to measured properties, the bridge is represented by microstructure; from the bridge to ranking criteria there is a need for normalization, application weighting, scoring, and decision boundaries evaluation. Placement of the diagram right after the description of the calculation algorithm allows for clear representation of the analysis flow prior to presenting its quantitative results.

This is evident from Figure 4 which shows that experimental data precede scoring while ranking and boundary calculation follow these steps. Such representation makes the analysis model more than a mathematical optimization approach and rather an engineering interpretation of the relationship between process-microstructure-mechanical properties.

3. Results

The results of comparing measured mechanical properties of the four candidate surface conditions are illustrated in Figure 5. It is essential that in this figure, prior to applying numerical weighing to the data, one can clearly see that the four candidate routes satisfy different mechanical requirements. Specifically, the M2 surface condition is the most rigid and shows minimal wear losses, carburized SCM420 shows excellent energy absorbing capacity, while Fe-8Cr-3V-2Mo-2W, post heat-treated, demonstrates the highest tensile strength. In addition, the Fe-8Cr-3V-2Mo-2W as-built condition is the weakest among the four, since in none of the four criteria does it take first place. In this way, it becomes obvious why a multi-objective decision-making scheme should be applied: it is impossible to choose the optimal surface treatment procedure based on just one characteristic.

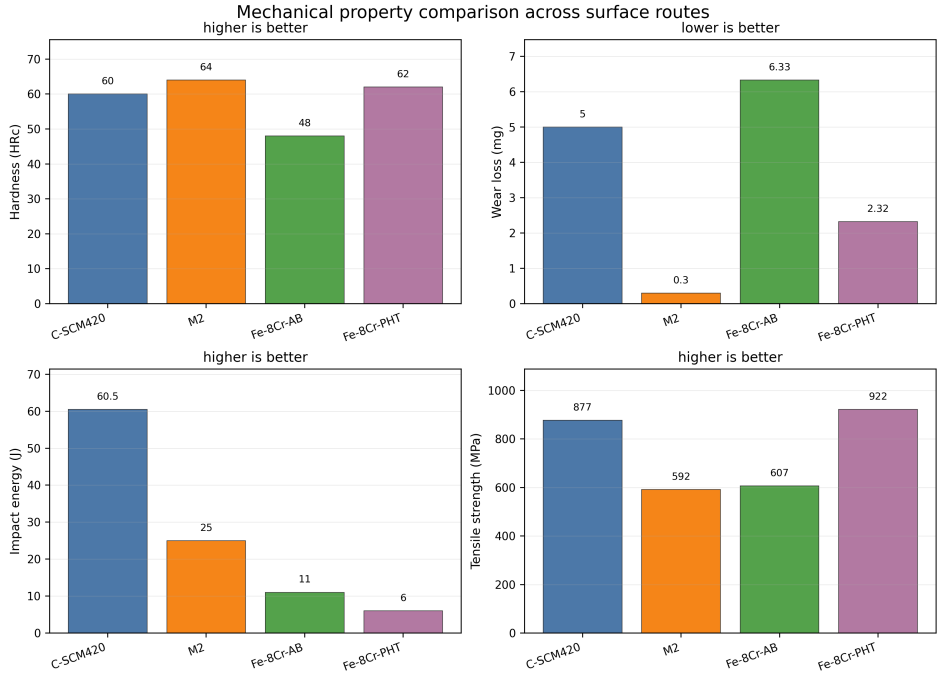

Figure 5. Mechanical-property comparison for the four candidate surface conditions using the values compiled in Table 4. The panel layout helps separate hardness, wear loss, impact energy, and tensile strength so that the main contrasts become evident before applying normalization and case-specific weighting.

It is obvious from Figure 5 that choosing any single criterion is inappropriate since M2 dominates in hardness and wear resistance, but not in tensile strength, while SCM420 dominates in impact energy but not in wear resistance; Fe-8Cr-3V-2Mo-2W provides both tensile strength and wear resistance.

3.1. Effect of post-heat treatment on the Fe-8Cr-3V-2Mo-2W deposit

In Table 7, one can see the quantitative assessment of how the post-heat treatment affects the Fe-8Cr-3V-2Mo-2W deposit. The heat treatment leads to 14 HRc increment in the hardness, which is equal to 29.2% growth compared to the as-built state. At the same time, wear loss is reduced from 6.33 mg to 2.32 mg or by 63.3%; the width of the wear track also reduces from 1030 μm to 798 μm or by 22.5%. Furthermore, the tensile strength rises by 315 MPa, or 51.9%. Thus, the post-heat treatment is a critical part of the process; it makes the alloy from as-built to mechanically superior hardfacing.

Table 7. Properties change caused by post-heat treatment of Fe-8Cr-3V-2Mo-2W deposit.

Criterion	As-built	Post-heat treated	Change
Hardness (HRc)	48	62	+14 (+29.2%)
Wear loss (mg)	6.33	2.32	-4.01 (-63.3%)
Wear track (μm)	1030	798	-232 (-22.5%)
Impact energy (J)	11.0	6.0	-5.0 (-45.5%)
Tensile strength (MPa)	607	922	+315 (+51.9%)

However, Table 7 shows an equally important aspect of the process. Post-heat treatment leads to a significant drop of 5.0 J (45.5%) in impact energy. It means that the effect of heat treatment is directional; on the one hand, it improves wear resistance and tensile strength and makes alloy harder, but, on the other hand, it reduces the ability of the material to absorb shock. The heat treatment causes the formation of the martensite-carbide structure; in such structures, cracking becomes easier under shock loads due to reduced resistance to plastic deformations.

Figure 6 shows the impact of the heat treatment on properties of the Fe-8Cr-3V-2Mo-2W deposit. One can clearly see the rise in hardness and tensile strength, and, at the same time, fall in wear loss and width of the wear track, which means that heat treatment improves these characteristics. However, the drop in absorbed impact energy is an important point because the choice between post-heat treated and non-post-heat treated material depends on this factor.

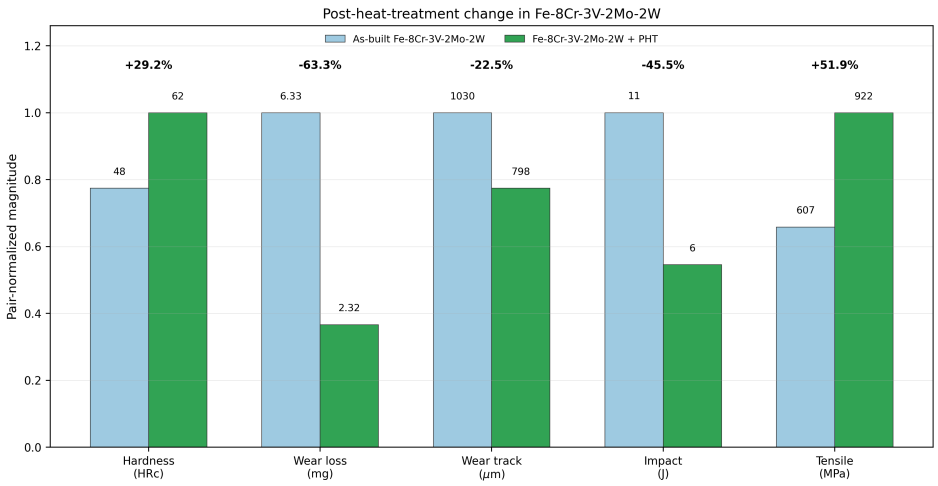

Figure 6. Direct effect of post-heat treatment on the Fe-8Cr-3V-2Mo-2W deposit. Pair-normalized bars are annotated with the measured values to show the simultaneous increase in hardness and tensile strength, decrease in wear loss and wear-track width, and reduction in absorbed impact energy.

As seen in Figure 6, the good and bad effects of treatments happen simultaneously. The significant decreases in both wear loss and wear track width reinforce the notion of increased surface resistance, whereas the decrease in impact energy suggests the inap-

propriateness of heat treatment in situations where loading and crack arrest ability are crucial.

3.2. Normalized desirability values and treatment-gain vector

The table of normalized desirability values shown in Table 8 is based on the values of constant factors in Table 6. The normalized matrix standardizes all of the material properties within a range between 0 to 1 but retains the direction toward optimization. In terms of hardness and wear desirability, as-built M2 achieves the highest value; carburized SCM420 attains the highest value for impact energy desirability; post-heat-treated Fe-8Cr-3V-2Mo-2W is highly desired in tensile desirability, and is also desirable in terms of hardness; its impact desirability, however, is zero since it has the smallest impact energy absorbed out of the four.

Table 8. Normalized desirability values calculated from the compiled dataset. Higher values indicate better performance.

Surface condition	Hardness	Wear	Impact	Tensile
C-SCM420	0.750	0.221	1.000	0.864
As-built M2	1.000	1.000	0.349	0.000
As-built Fe-8Cr-3V-2Mo-2W	0.000	0.000	0.092	0.045
Fe-8Cr-3V-2Mo-2W + PHT	0.875	0.665	0.000	1.000

An additional useful vector is the normalized treatment-gain vector between the two states of Fe-8Cr-3V-2Mo-2W, as-built and post-heat-treatment:

$$\Delta \mathbf{z}_{\mathrm{PHT-AB}} = [0.875,\ 0.665,\ -0.092,\ 0.955]_{H,W,I,T}. \tag{10}$$

As seen from Eq. (10), the greatest normalized gain in this case is in tensile strength, followed by hardness and wear desirability. In spite of being small in absolute magnitude, the negative impact value is important for the decision-making, since the absorbed impact energy criterion is the dominant criterion of choice in a shock-sensitive application domain. Eq. (10) provides an intuitive understanding of why post-heat treatment can be quite beneficial in structural hardfacing but detrimental for impact-related duties.

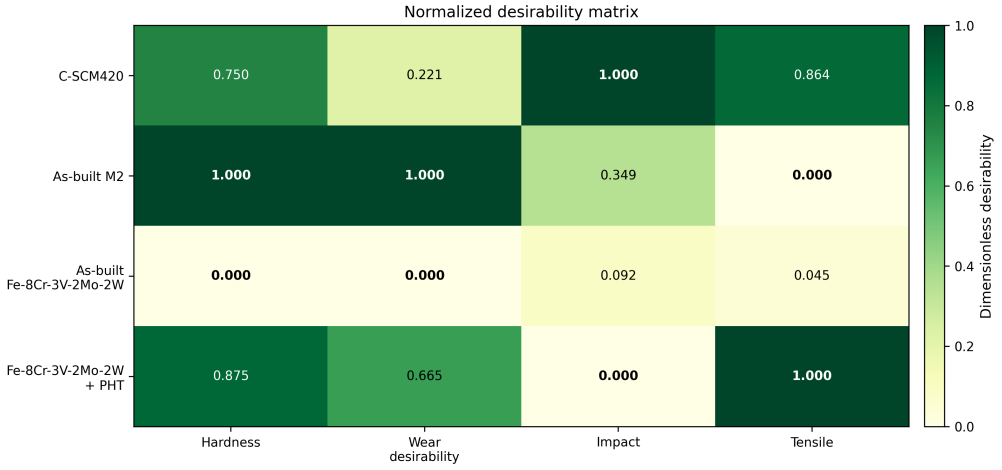

Figure 7. Normalized desirability matrix, estimated from the collected data by means of Eqs (1) and (2). High values correspond to better performance after properties have been adjusted into a dimensionless form.

Finally, the desirability matrix is also visualized in Figure 7. As one can see from the corresponding heatmap, there is no globally dominating surface candidate material, which confirms our initial assumption. For instance, while M2 is a good material from the

standpoint of tribological performance, carburized SCM420 is a good impact absorber, and post-heat-treated Fe-8Cr-3V-2Mo-2W is a strength dominating material. Therefore, a route selection is a problem of optimal allocation of different material properties within certain limits of acceptable performance, which cannot be achieved by simply choosing one best material.

The heatmap clearly shows that there is a problem with the compensations made. Post-treated Fe-8Cr-3V-2Mo-2W lies in the high-strength/high-hardness area of the matrix, while its impact cell is zero; thus, the route may result in only the tasks, in which impact energy absorption does not play a dominant role. Such an explanation of results corresponds to the gain vector presented in Eq. (10).

3.3. Service-specific score rankings

Weighted scores for the three types of service are presented in Table 9. Ranking of candidates in case of wear dominance in tooling use is as follows: As-built M2 > Fe-8Cr-3V-2Mo-2W + PHT > C-SCM420 > As-built Fe-8Cr-3V-2Mo-2W. Impact-dominant ranking is as follows: C-SCM420 > As-built M2 > Fe-8Cr-3V-2Mo-2W + PHT > As-built Fe-8Cr-3V-2Mo-2W. Balanced structural-hardfacing application ranking: Fe-8Cr-3V-2Mo-2W + PHT > As-built M2 > C-SCM420 > As-built Fe-8Cr-3V-2Mo-2W.

Table 9. Application-specific ranking scores calculated using the weighted-sum model.

Surface condition	Wear-dominant	Impact-dominant	Structural hardfacing
C-SCM420	0.522	0.870	0.624
As-built M2	0.835	0.409	0.635
As-built Fe-8Cr-3V-2Mo-2W	0.014	0.064	0.023
Fe-8Cr-3V-2Mo-2W + PHT	0.695	0.354	0.752

The score difference helps in evaluating the extent of the preference. For the wear-dominant tooling scenario, M2 has an advantage over the post-treated Fe-8Cr-3V-2Mo-2W alloy of 0.140 score points; hence, M2 is favored by its superior wear desirability score under abrasion-dominated service even after taking account of its inferior impact rating. In impact-controlled application, carburized SCM420 scores 0.516 more score points than the post-treated Fe-8Cr-3V-2Mo-2W deposit; thus, M2 cannot compete under impact-dominated service due to its relatively weak impact score. For the hardfacing application, where wear and strength equally contribute, post-treated Fe-8Cr-3V-2Mo-2W scores 0.117 higher than M2, while it scores 0.128 better than C-SCM420.

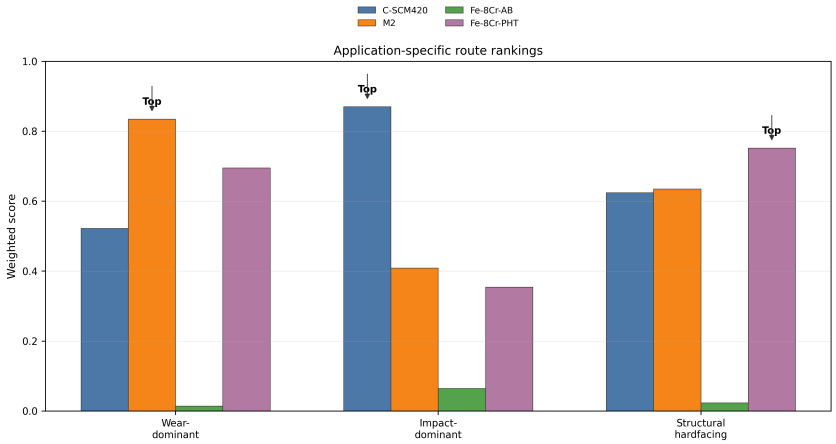

Figure 8. Application-specific weighted scores for the four candidate routes under wear-dominant tooling, impact-dominant duty, and balanced structural-hardfacing conditions. The top marker in each group identifies the preferred route produced by the score matrix in Table 9.

Figure 8 provides a visual representation of the above results. It can be observed from the graph that preference for one route over another depends on the nature of duty. This is the primary result derived through the methodology applied within the manuscript; that is, each of the three selected routes is optimal in a certain region of service space.

Figure 8 is the key graph in the manuscript since it clearly shows how the optimal route changes as a function of duty requirements. Specifically, the figure illustrates that the optimum route shifts from M2 to carburized SCM420, and eventually to post-treated Fe-8Cr-3V-2Mo-2W as the nature of service evolves from abrasion resistance to shock resistance and finally to balanced wear-strength resistance.

3.4. Criterion-level score contributions

In order to understand the reason for a particular candidate's success or failure, Table 10 breaks down the balanced structural-hardfacing score into its respective criteria scores. The post-heat-treated Fe-8Cr-3V-2Mo-2W condition scores 0.219 on hardness, 0.233 on wear resistance, 0.000 on impact toughness, and 0.300 on tensile strength. This result shows that the balanced structural-hardfacing score is not a toughness score, but rather a composite of hardness, wear, and strength scores. The M2 condition gets a good score of 0.600 in hardness and wear resistance combined, but scores nothing on tensile strength since it has the lowest tensile strength among all candidates in the normalized set. The C-SCM420 scores highly on both impact toughness and tensile strength, but scores poorly on wear desirability.

Table 10. Criterion-level score contributions for the balanced structural-hardfacing case.

Surface condition	Hardness	Wear	Impact	Tensile	Total
C-SCM420	0.188	0.077	0.100	0.259	0.624
As-built M2	0.250	0.350	0.035	0.000	0.635
As-built Fe-8Cr-3V-2Mo-2W	0.000	0.000	0.009	0.014	0.023
Fe-8Cr-3V-2Mo-2W + PHT	0.219	0.233	0.000	0.300	0.752

The significance of this decomposition lies in the fact that it guards against overstating the Fe-8Cr-3V-2Mo-2W heat-treated path. Although its superiority with respect to structure-hardfacing does not imply that it is well-balanced in mechanical terms, it implies that the increase in strength and wear resistance is sufficient to counterbalance the impact decrement with respect to the structural-hardfacing weights chosen. In an application where impact energy is a qualification criterion, the above path would have to be subjected to further process optimization or even changed altogether.

3.5. Decision-boundary analysis between the competing paths

Pairwise difference scores were read off the desirability matrix for Fe-8Cr-3V-2Mo-2W post-heat treatment and M2 as-built.

$$\Delta S_{\mathrm{PHT-M2}} = -0.125 w_H - 0.335 w_W - 0.349 w_I + 1.000 w_T. \tag{11}$$

Thus, post-heat-treated Fe-8Cr-3V-2Mo-2W outranks M2 when

$$w_T > 0.125 w_H + 0.335 w_W + 0.349 w_I. \tag{12}$$

As seen from Eqs. (11) and (12), PHT Fe-8Cr-3V-2Mo-2W can surpass M2 only if the weight of tensile strength is sufficiently high so as to offset the superior hardness, wear resistance, and impact resistance of M2. Using the ratio of structural-to-hardfacing weights adopted in this case, the critical value for tensile strength is about 0.208; the chosen weight of 0.300 is thus well within the PHT-advantaged region.

For post-heat-treated Fe-8Cr-3V-2Mo-2W versus carburized SCM420,

$$\Delta S_{\mathrm{PHT-C}} = 0.125 w_H + 0.444 w_W - 1.000 w_I + 0.136 w_T. \tag{13}$$

Thus, post-heat-treated Fe-8Cr-3V-2Mo-2W beats carburized SCM420 if

$$w_I < 0.125w_H + 0.444w_W + 0.136w_T. \tag{14}$$

It has an easily understood physical explanation. After impact is given a very high weight, carburized SCM420 wins again due to the much larger energy absorbed in its composite microstructure. At constant proportions of non-impact structural weights as that in the structural-hardfacing case, the critical weight of impact is about 0.202. The selected weight for structural-hardfacing case of 0.100 is less than this critical value, while the case where impact dominates uses 0.600, selecting carburized SCM420.

In comparing M2 with carburized SCM420,

$$\Delta S_{\mathrm{M2-C}} = 0.250w_H + 0.779w_W - 0.651w_I - 0.864w_T. \tag{15}$$

M2 is therefore preferred when the combined importance of hardness and wear exceeds the combined advantage of SCM420 in impact and tensile performance. Table 11 summarizes the resulting boundaries.

Table 11. Pairwise decision boundaries among the three competitive top-ranked routes.

Comparison	Condition for the first route to rank higher
PHT vs. M2	$w_T > 0.125w_H + 0.335w_W + 0.349w_I$
PHT vs. C-SCM420	$w_I < 0.125w_H + 0.444w_W + 0.136w_T$
M2 vs. C-SCM420	$0.250w_H + 0.779w_W > 0.651w_I + 0.864w_T$

Indeed, the decision boundaries prove the conditionality of the post-heat-treated Fe-8Cr-3V-2Mo-2W option. The alloy stands out whenever wear-resistance and tensile strength characteristics are important at once, but it falls behind M2 when wear characteristics prevail and falls behind carburized SCM420 if impact-absorption characteristics prevail. Figure 9 summarizes these inequalities as pairwise differences between the options under the service weights.

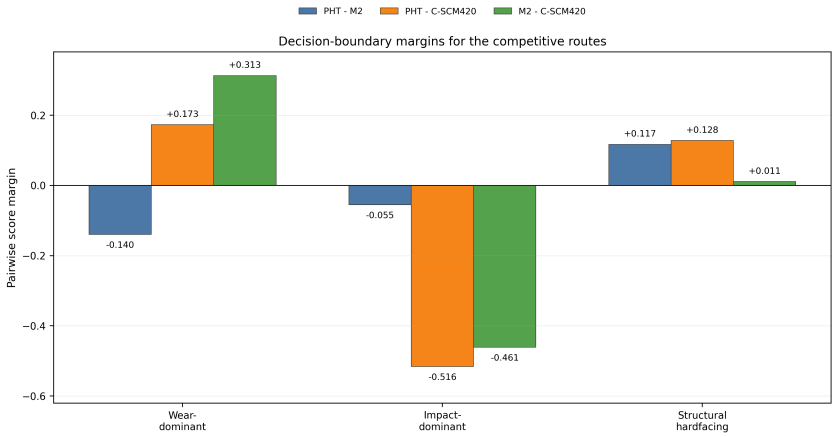

Figure 9. Margin chart based on the decision boundaries for the three competing options. Positive bars show that the first named option in the legend is better than the second option under the respective service weights, while negative bars show vice versa.

It can be observed from the margin chart how analytically established inequalities hold visually as well. In particular, the negative PHT–M2 bar proves that M2 is still leading when the weight of wear is predominant, while the positive M2–C-SCM420 bar proves that tribological consideration is more important for high-speed-steel deposition. Moreover, in the case of impact domination, both PHT–C-SCM420 and M2–C-SCM420 margins are negative, thus confirming the leading position of carburized SCM420 option in the shock

sensitive region. Finally, when considering the structural hardfacing application, both PHT–M2 and PHT–C-SCM420 margins turn positive.

3.6. Verification of distance to ideal

The weighted closeness index to the ideal solution is presented in Table 12. Consistently with previous results, the closeness index identifies exactly the same alternative route as the closest to the ideal one in all service cases: M2 is the closest one among wear-dominant alloys, carburized SCM420 is the closest in case of impact-dominant surface loading conditions, and post-heat-treated Fe-8Cr-3V-2Mo-2W is the closest when structural hardfacing is the key criterion. This is a significant point as this result shows that the ranking is not based solely on the weighted linear sum.

Table 12. Closeness index to the weighted ideal solution for the three surface conditions.

Surface condition	Wear-dominant	Impact-dominant	Structural hardfacing
C-SCM420	0.516	0.772	0.589
As-built M2	0.705	0.437	0.572
As-built Fe-8Cr-3V-2Mo-2W	0.032	0.073	0.038
Fe-8Cr-3V-2Mo-2W + PHT	0.649	0.420	0.680

In addition to highlighting the closeness of some alternatives, the distance-based values indicate that some alternatives are closer. For instance, in the wear-dominant scenario, M2 continues to be preferred over post-heat-treated Fe-8Cr-3V-2Mo-2W with a closeness value of 0.056. Similarly, in the impact-dominant scenario, carburized SCM420 is clearly preferred, demonstrating a strong preference. In the structural hardfacing scenario, on the other hand, post-heat-treated Fe-8Cr-3V-2Mo-2W is favored over M2 and C-SCM420. This supplementary indicator, therefore, confirms the finding that the heat-treated Fe-8Cr-3V-2Mo-2W alternative represents a unique structural-wear design opportunity as opposed to a marginal option.

3.7. Discussion

A route-selection calculation clearly reveals an engineering interpretation of the four candidate surface routes beyond property comparison. The as-built Fe-8Cr-3V-2Mo-2W deposit has the worst desirability indices for structural hardfacing due to the fact that its microstructure has not attained the level of hardening by martensite formation and carbide precipitation required for effective resistance to wear and tensile loading. Thus, the poor desirability of this route does not originate from the scoring scheme but reflects actual engineering reality: Fe-8Cr-3V-2Mo-2W can hardly be considered as a usable hardfacing material in the as-deposited state.

The M2 route demonstrates the other extreme. It is highly specialized for wear-dominated tooling service because it offers the maximum hardness and minimum wear loss. The contribution of hardness-wear term to the score value of this route is confirmed by the score decomposition table. However, the same table explains why M2 cannot compete with carburized SCM420 under structural hardfacing: its tensile score value equals zero. This example demonstrates that the material that is best for wear-dominated tooling will not necessarily be the best for load-bearing hardfacing.

Carburized SCM420 is still the most reliable route for impact-dominated tooling. Unlike the deposited material whose ability to resist loads depends only on surface hardening, the case/core architecture of carburized steel makes it able to absorb larger amounts of energy until the critical failure point. Consequently, impact- and distance-to-ideal-based scores indicate that carburized SCM420 is the most effective impact-resistant material among candidates because its energy absorption is maximally distant from the critical impact value.

As was already mentioned above, the most notable result is obtained for the heat-treated Fe-8Cr-3V-2Mo-2W deposit. It is not the best option for wear-dominant service

because the other candidates offer comparable properties, and it fails to compete with carburized SCM420 under impact. Its unique advantage is associated with the fact that it is the best route when a load-bearing deposited surface is subject to combined wear and tensile duty. The heat-treated Fe-8Cr-3V-2Mo-2W route has very good score values for hardness, wear, and tensile strengths; its desirability indices equal 0.875, 0.665, and 1.000 respectively. Hence, this route yields the maximum structural hardfacing score (1.410) and the maximum structural closeness to ideal (0.581). Despite its relatively bad impact desirability (zero), which is a crucial property of this material, this factor cannot affect the selection as long as the impact-dominated duty is not emphasized.

The mathematical derivation of scores and desirability indices provided several benefits for design purposes. First of all, normalized coefficients explicitly reveal the criteria scales used during scoring. The second benefit is represented by score contribution tables; they explain the nature of each selected candidate and prevent reduction of selection conclusion to numbers. Finally, the decision-boundary formulas allow a designer to predict whether a particular selection is valid at any weight ratio without re-calculation of a new candidate scoring table.

The threshold values are especially useful because they provide a basis for further design considerations. Under the selected structural weight ratio ($w_t/(w_h + w_w) = 1/2$), Fe-8Cr-3V-2Mo-2W requires $w_t > 0.208$ to dominate M2, which implies that the selected ratio of 0.300 provides sufficient emphasis on hardness and tensile strength. However, if the proportions of two non-impact criteria are preserved, then the selected impact weight must not exceed 0.202 for Fe-8Cr-3V-2Mo-2W to outrank carburized SCM420. As the selected value of 0.100 is less than 0.202, it is sufficiently low to select Fe-8Cr-3V-2Mo-2W. The value of 0.600 used for impact-dominated service, however, does not satisfy this condition.

Another robustness check of the selected candidates is provided by distance-to-ideal calculations. Indeed, a weighted-score may occasionally show some candidate as better because of very high values of one criterion, despite that the general properties' profile is far away from the optimum. In the current study, distance-to-ideal scores are in agreement with weighted sums: the best options for all service cases are identified in the same way.

M2 is the best score value and the closest ideal candidate for wear-dominant tooling, the same is true for carburized SCM420 under impact-dominant service and Fe-8Cr-3V-2Mo-2W under structural hardfacing.

The post-heat-treated microstructure of the Fe-8Cr-3V-2Mo-2W deposit should be analyzed carefully. Hardness and tensile-strength improvement is possible if a layer's microstructure includes less retained austenite and more hardening elements in the form of martensite. In addition, the reduction of impact energy proves that the developed structure is also characterized by increased brittleness; in the case of deposited materials, carbides, brittle regions and cracks, local residual stresses and pores can be among such factors. Therefore, one should not consider Fe-8Cr-3V-2Mo-2W as an exceptionally tough material.

The post-heat-treated layer of Fe-8Cr-3V-2Mo-2W is especially useful for repairing and reinforcing mechanical components where the deposited surface needs to bear loads. Such examples include locally reinforced shafts, restored sliding surfaces and worn areas, surfaces of tools subjected to combined contact and tensile stresses, etc. In those cases, a purely wear-optimized deposited material cannot solve the problem. Moreover, a carburized route, which is designed to be impact-resistant, is likely to be unable to withstand the progressive wear. In those circumstances, Fe-8Cr-3V-2Mo-2W seems to be the best choice among candidates.

Despite all these limitations, this research makes a contribution in the field of mechanical engineering because of several reasons. Firstly, the conversion of a comparison based on numerical data to route-selection with emphasis on engineering criteria is provided. Secondly, the physical sense of selected routes and mechanisms of their scoring are explained. Finally, the derived formulae for recalculation of preferred routes under changed weight ratio are provided.

4. Conclusions

A number of mechanical conclusions can be drawn from the Fe-8Cr-3V-2Mo-2W hardfacing comparison. Heat-treatment improves the competitive condition of Fe-8Cr-3V-2Mo-2W significantly. After heat-treatment, its hardness goes up from 48 to 62 HRc, its wear loss drops from 6.33 to 2.32 mg, wear-track width falls from 1030 to 798 μm, and its tensile strength increases from 607 to 922 MPa. Meanwhile, the heat-treatment effect is manifested through decreased impact energy absorption, from 11 to 6 J – this means that the mechanical effects of the treatment are directional rather than universal. This is corroborated by the normalized treatment-gain vector, $\Delta\mathbf{z} * \mathrm{PHT} - \mathrm{AB} = [0.875, 0.665, -0.092, 0.955] * H, W, I, T$, that reveals tensile strength as a field where the greatest improvement due to treatment is achieved; second to tensile strength, there are gains in hardness and wear desirability. The negative sign of the impact component proves the necessity of restricting the heat-treatment process application scope to those applications where impact protection does not have priority. As-built M2 should remain a preferred option for designing wear-dominant tooling because it possesses higher hardness and greater wear desirability despite being inferior to heat-treated Fe-8Cr-3V-2Mo-2W in terms of tensile strength, especially taking into account that the latter is not a primary concern in designing wear-resistant tools.

On the other hand, carburized SCM420 can remain a preferred route in case of impact-dominance design criterion because its case-core structure provides for much higher impact energy absorption than any deposited solution. As a result, it provides a clear advantage in terms of mechanical performance at shock-sensitivity weighting. Heat-treated Fe-8Cr-3V-2Mo-2W can be identified as a candidate for structural hardfacing with the most effective structural score: 0.752, that exceeds M2 score by 0.117 units and carburized SCM420 one by 0.128 – that is possible thanks to its high hardness, increased wear resistance, and the highest tensile strength. Further criterion-level score breakdown analysis shows that the structural advantage of the heat-treated Fe-8Cr-3V-2Mo-2W route is mostly attributed to tensile and wear strength and not to impact tolerance. This helps to avoid overgeneralization. Accordingly, the decision boundary equations suggest that the heat-treated Fe-8Cr-3V-2Mo-2W outranks M2 provided the tensile-weight parameter is larger than 0.208 and outpaces carburized SCM420 when the impact-energy weight stays below a critical level: $w_I < 0.202$. The same values apply to the chosen structural weighting ratio. The weighted distance-to-ideal diagnostic tool supports the above-mentioned conclusion on the preferred route depending on the criterion weighting order. According to it, M2 represents the closest-to-ideal solution for wear-dominant tooling; carburized SCM420 is closest in case of impact-dominant criteria weighting; heat-treated Fe-8Cr-3V-2Mo-2W wins in balanced structural criteria case. Therefore, the Fe-8Cr-3V-2Mo-2W alloy system should be recognized as targeted DED hardfacing rather than a substitute for the other two materials. Future material qualification should include considerations of fatigue, residual stress, porosity, fracture toughness, and non-compensatory constraint screening in the current selection process.

Nomenclature

DED	Directed energy deposition
PHT	Post-heat treatment
HRc	Rockwell hardness, C scale
H	Hardness criterion
W	Wear desirability criterion
I	Impact-energy criterion
T	Tensile-strength criterion
x_{ij}	Measured value of candidate i under criterion j
z_{ij}	Normalized desirability of candidate i under criterion j
w_j	Weight assigned to criterion j
q_{ij}	Weighted contribution of criterion j to candidate i

S_i	Application-specific service score of candidate i
ΔS_{A-B}	Pairwise score margin between candidates A and B
d_i^+	Weighted distance from the positive ideal property vector
d_i^-	Weighted distance from the negative ideal property vector
C_i	Weighted distance-to-ideal closeness index

Data Availability

The numerical inputs used in the multi-objective analysis are the measured values tabulated by Jeong et al. for the four compared surface conditions [15].

References

[1] ASM International. (1992). *ASM Handbook, Volume 18: Friction, Lubrication, and Wear Technology*. ASM International.

[2] Herzog, D., Seyda, V., Wycisk, E., & Emmelmann, C. (2016). Additive manufacturing of metals. *Acta Materialia*, 117, 371–392.

[3] Lewandowski, J. J., & Seifi, M. (2016). Metal additive manufacturing: a review of mechanical properties. Annual review of materials research, 46(1), 151-186.

[4] Mazumder, J., Dutta, D., Kikuchi, N., & Ghosh, A. (2000). Closed loop direct metal deposition: Art to part. *Optics and Lasers in Engineering*, 34(4–6), 397–414.

[5] Pinkerton, A. J., Wang, W., & Li, L. (2008). Component repair using laser direct metal deposition. *Proceedings of the Institution of Mechanical Engineers, Part B: Journal of Engineering Manufacture*, 222(7), 827–836.

[6] DebRoy, T., Wei, H. L., Zuback, J. S., Mukherjee, T., Elmer, J. W., Milewski, J. O., ... & Zhang, W. (2018). Additive manufacturing of metallic components–process, structure and properties. Progress in materials science, 92, 112-224.

[7] Li, S. H., Kumar, P., Chandra, S., & Ramamurty, U. (2023). Directed energy deposition of metals: processing, microstructures, and mechanical properties. International Materials Reviews, 68(6), 605-647.

[8] Wang, S. H., Chen, J. Y., & Xue, L. (2006). A study of the abrasive wear behaviour of laser-clad tool steel coatings. *Surface and Coatings Technology*, 200(11), 3446–3458.

[9] Leunda, J., Soriano, C., Sanz, C., & Navas, V. G. (2011). Laser cladding of vanadium-carbide tool steels for die repair. Physics Procedia, 12, 345-352.

[10] Rahman, N. U., Capuano, L., Van der Meer, A., De Rooij, M. B., Matthews, D. T. A., Walmag, G., ... & Römer, G. R. B. E. (2018). Development and characterization of multilayer laser cladded high speed steels. Additive Manufacturing, 24, 76-85.

[11] Rahman, N. U., Capuano, L., Cabeza, S., Feinaeugle, M., Garcia-Junceda, A., De Rooij, M. B., ... & Römer, G. R. B. E. (2019). Directed energy deposition and characterization of high-carbon high speed steels. Additive Manufacturing, 30, 100838.

[12] Ashby, M. F., Brechet, Y. J. M., Cebon, D., & Salvo, L. (2004). Selection strategies for materials and processes. *Materials & Design*, 25(1), 51–67.

[13] Ashby, M. F. (2011). *Materials Selection in Mechanical Design* (4th ed.). Butterworth-Heinemann.

[14] Athawale, V. M., & Chakraborty, S. (2012). Material selection using multi-criteria decision-makireng methods: a comparative study. Proceedings of the Institution of Mechanical Engineers, Part L: Journal of Materials: Design and Applications, 226(4), 266-285.

[15] Jeong, Y. E., Lee, J. Y., Lee, E. K., & Shim, D. S. (2021). Microstructures and mechanical properties of deposited Fe-8Cr-3V-2Mo-2W on SCM420 substrate using directed energy deposition and effect of post-heat treatment. Materials, 14(5), 1231.

[16] Shim, D. S., Baek, G. Y., Lee, S. B., Yu, J. H., Choi, Y. S., & Park, S. H. (2017). Influence of heat treatment on wear behavior and impact toughness of AISI M4 coated by laser melting deposition. Surface and Coatings Technology, 328, 219-230.

[17] Baek, G. Y., Shin, G. Y., Lee, K. Y., & Shim, D. S. (2020). Effect of post-heat treatment on the AISI M4 layer deposited by directed energy deposition. Metals, 10(6), 703.

[18] Yadav, S., Dileep, K., Jinoop, A. N., Paul, C. P., Rai, A. K., Singh, R., & Bindra, K. S. (2023). Laser directed energy deposition of high-carbon high-chromium D2 tool steel structures: processing, heat treatment and material behavior. Journal of Materials Engineering and Performance, 32(11), 4881-4891.

[19] Hwang, C. L., & Yoon, K. (1981). *Multiple Attribute Decision Making: Methods and Applications*. Springer.

[20] Shanian, A. A., & Savadogo, O. (2006). A material selection model based on the concept of multiple attribute decision making. Materials & Design, 27(4), 329-337.

[21] Rao, R. V. (2007). Decision making in the manufacturing environment: using graph theory and fuzzy multiple attribute decision making methods. London: Springer London.